Journal of Materials Chemistry A

Accepted Manuscript

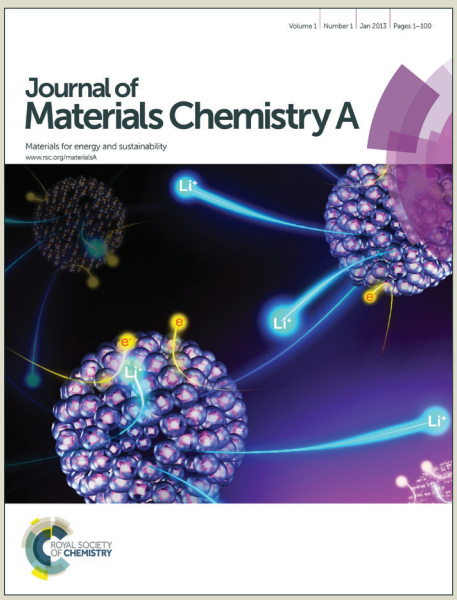

ROYAL SOCIETY OF CHEMISTRY

www.rsc.org/materialsA

Journal of

Materials Chemistry A

RSCPublishing

Paper

Manipulating the interfacial interactions of composite membrane via mussel-inspired approach toward enhanced separation selectivity

Cite this: DOI: 10.1039/x0xx00000x

Received 00th January 2012,
Accepted 00th January 2012

DOI: 10.1039/x0xx00000x

www.rsc.org/

Jing Zhao,[a,b] Chenhao Fang,[a,b] Yiwei Zhu,[a,b] Guangwei He,[a,b] Fusheng Pan,[a,b] Zhongyi Jiang,*[a,b] Peng Zhang,[c,d] Xingzhong Cao[c,d] and Baoyi Wang[c,d]

For the broadly utilized composite membrane with dense separation layer and porous support layer, the rational manipulation of interfacial interactions between these two layers is vital to optimize membrane structure and the associated performance. In this study, we report a facile mussel-inspired approach to enhancing separation selectivity of composite membrane by co-depositing biomimetic adhesive dopamine and poly(ethylene imine) (PEI) on support layer, and then coating sodium alginate (SA) as separation layer. PEI is anchored onto support layer surface through the reaction with dopamine during polydopamine (PDA) formation process, thus incorporating electrostatic attraction interaction into the interface besides the hydrogen bond interaction between PDA and SA. Using water/alcohol separation as the model system, the separation factor of SA/PEI-PDA/PAN membrane can reach 1807, which is 29.6 and 6.8-fold higher than those of SA/PAN and SA/PDA/PAN membranes, respectively. The remarkably enhanced separation factor arises from the optimal free volume property and swelling resistance of membrane under the optimized interfacial interactions between separation layer and support layer. This study may present an efficient and facile approach to tailoring membrane structure for enhanced separation performance.

1. Introduction

To simultaneously achieve high separation performance and good stability, composite membrane with dense separation layer and porous support layer is an ingenious configuration in many membrane applications ranging from industrial-scale carbon capture, biofuel production and seawater desalination to smaller-scale chemical purification.[1-4] However, the long-term utilization of composite membrane has been severely impeded by the low interfacial bonding strength between separation layer and support layer, which is attributed to the interfacial stress induced by the discrepancy of swelling property.[5-7] Furthermore, the assembly of polymer chains into separation layer during membrane formation process is dramatically affected by the interfacial interactions between these two layers through interfacial cross-linking.[8] Therefore, interfacial interaction manipulation is recognized as a vital strategy for composite membrane to optimize membrane structure and the associated performance.[5, 8-10] The commonly utilized manipulation approaches focus on surface modification of support layer before depositing separation layer, including surface chemical/physical treatment[11], etc. In comparison, the biomimetic adhesion inspired by the adhesive behaviour of mussels affords an innovative surface modification method for support layer with distinct superiorities including mild condition, easy operation, excellent wet-adhesion capacity and exceptional universality.[12-15] Biomimetic adhesives, bearing similar chemical structure with the functional constituent in mussel adhesive protein (catecholamines), have performed robust and non-specific adhesion on diverse substrates ranging from organic to inorganic, hydrophilic to hydrophobic, planar to nonplanar, and have found applications in various membrane processes.[9, 10, 16-18]

Although biomimetic adhesion has been demonstrated as a versatile surface modification approach, there are still some critical issues to be solved when manipulating interfacial interactions for enhanced performance of composite membrane. (1) The insufficient interfacial bonding strength between separation layer and biomimetic adhesive-modified support layer. As is well known, the biomimetic adhesive possesses chemical versatility to generate multi-level interactions such as covalent bond, metal chelation, hydrogen-bond, and π-π interaction with membrane materials.[15, 19] However, the formation of strong interactions relies on specific chemical structures such as the nucleophilic amine/thiol groups for

covalent bond[20], and the metals/metal oxides for metal chelation[20, 21]. This greatly restricts its applicability in membrane materials lacking of the above mentioned chemical structures. (2) The limited application range of manipulating interfacial bonding strength. Although biomimetic adhesion process can be regulated by pH, temperature, concentration, etc.,[19, 22] the interfacial bonding strength between separation layer and biomimetic adhesive-modified support layer is governed by the adhesion/cohesion balance of biomimetic adhesive: the adhesive energy and cohesive energy of biomimetic adhesive are often in tradeoff relation, whereas both of them contribute to the interfacial bonding strength.[12, 23]

To address these two issues, incorporation of an adjuvant adhesive during biomimetic adhesion process bearing the matched chemical structure with separation layer material seems an ingenious strategy. In this study, poly(ethylene imine) (PEI) was co-deposited on support layer with biomimetic adhesive dopamine (DA) before coating sodium alginate (SA) as separation layer. The deposition of PEI molecules along with dopamine is achieved through the covalent reaction between PEI and dopamine during the formation process of polydopamine (PDA). As a result, electrostatic attraction interaction between positively charged PEI and negatively charged SA is imported into the separation layer-support layer interface along with the hydrogen bond interaction between PDA and SA. Additionally, the interfacial bonding strength can be conveniently manipulated through regulating deposition conditions including PEI/DA mass ratio and deposition time to tune the adhesion/cohesion balance of PDA as well as the final PEI/PDA mass ratio on support layer surface. Water/alcohol separation was employed as a model system to investigate the influence of manipulating interfacial interactions between separation layer and support layer on separation performance of as-fabricated composite membranes.

2. Experiment

2.1. Materials

Sodium alginate (SA) was supplied by Qingdao Bright Moon Seaweed Group Co. Ltd. (Shandong, China). Dopamine hydrochloride was purchased from Wuhan Yuancheng Technology Development Co., Ltd. (Hubei, China). Polyethyleneimine (PEI, Mw=1800 Da) and Tris were supplied by Sigma-Aldrich (USA). The flat-sheet polyacrylonitrile (PAN) ultrafiltration membrane with a molecular weight cut-off of 100 000 was received from Shandong MegaVision Membrane Technology & Engineering Co. Ltd. (Shandong, China). Hydrochloric acid (HCl, 36-38 wt%) was purchased from Tianjin Kewei Ltd. (Tianjin, China). Ethanol (≥ 99.7 wt%) was received from Tianjin Guangfu Fine Chemical Research Institute (Tianjin, China). All the reagents were of analytical grade and used as received. Deionized water was used throughout the experiments.

2.2. Membrane fabrication

The fabrication procedures of composite membranes are briefly illustrated in Scheme 1. The deposition of PDA or PEI-PDA on PAN membrane and the sequent coating of SA were performed employing a home-made single-side dip-coating device to avoid the deposition of PDA and PEI on the polyester back side of PAN membrane.[24] First, the PAN membranes were soaked in ethanol for prewetting before being fixed in the dip-coating device. Afterwards, tris-buffer solution (50 mM, pH = 8.5) dissolving 2 mg/mL of dopamine hydrochloride and a certain amount of PEI was prepared and poured into the device. The device was put on a vapour-bathing constant temperature vibrator to achieve vibration and constant temperature at 25 ^{o}C during the PDA or PEI-PDA deposition process. After a predetermined time, the surface-modified PAN membranes were rinsed with deionized water and dried at room temperature. SA was dissolved in water with a concentration of 5 mg/ml. After stirring for 24 h, SA solution was poured into the device and kept still for 1 min before pour-out. The ultimate membranes were obtained after drying at room temperature. The resultant membranes were designated as SA/PEI-PDA(X, Y)/PAN, where X represented the deposition time of PDA or PEI-PDA (0 h, 2 h, 4 h, 8 h, 16 h), Y represented the mass ratio of PEI to DA (0:1, 0.5:1, 1:1, 2:1). The membrane with mass ratio of 0:1 and deposition time of 4 h was simplified as SA/PDA(4 h)/PAN, and the membrane with deposition time of 0 h was simplified as SA/PAN. The membranes without SA were fabricated for characterizations and designated as PEI-PDA(X, Y)/PAN.

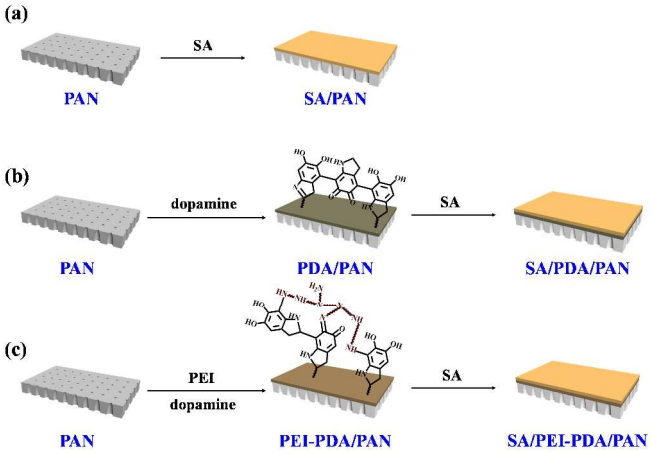

Scheme 1. Fabrication procedures of composite membranes: (a) SA/PAN membrane fabricated through SA coating, (b) SA/PDA/PAN membrane fabricated through PDA deposition and SA coating, (c) SA/PEI-PDA/PAN membrane fabricated through PEI-PDA deposition and SA coating.

2.3. Membrane characterizations

The surface and cross-section morphologies of membrane were observed by field emission scanning electron microscope (FESEM) (Nanosem 430). FTIR spectra of membranes in the range of 4000-500 cm^{-1} were recorded on a BRUKER Vertex 70 FT-IR spectrometer equipped with a horizontal attenuated total reflectance accessory. The chemical compositions of deposited PEI-PDA under different conditions were measured by an elemental analyzer (vario EL CUBE) to ascertain the final PEI/PDA mass ratio on support layer surface. The surface charge properties of PEI-PDA/PAN membranes were characterized by a zeta-potential analyzer (Anton Paar SurPASS) with 1 mmol/L KCl (pH = 7.0 ± 0.2) as electrolyte solution. The surface hydrophilicity of PEI-PDA/PAN membranes was evaluated by measuring the static water contact angle at room temperature with a contact angle goniometer (JC2000C Contact Angle Meter). The free volume properties at various depths of the composite membranes were characterized by positron annihilation technology. The positrons implanted into the membrane will annihilate upon encountering electrons in membrane, and release γ photons, which indicate the information of cavities in the locations where positrons annihilate. The different energies of implanted positrons correspond to different positron implantation depths. Slow positron annihilation Doppler broadening spectra were obtained with the energy of implanted positrons continuously varying in the range of 0.18–20 keV. ^{22}Na radioactive source and high-purity Ge detector were utilized.

2.4. Membrane separation experiment

In this study, the separation performance of as-fabricated composite membranes was evaluated utilizing the pervaporation dehydration of ethanol aqueous solution as a model system.

Pervaporation experiments were performed with the P-28 membrane module (CM-Celfa AG Company, Switzerland). The effective membrane area in contact with feed solution was 25.6 cm^2. The down-stream pressure of membrane was kept below 0.3 kPa using a vacuum pump, and the flow rate of feed solution was controlled at 60 L/h. The permeate was collected with a cold trap immersed in liquid nitrogen and taken out at a fixed interval. The mass of permeate solutions were weighted. The compositions of feed and permeate solutions were determined by gas chromatography (Agilent 7820A, USA). The separation performance of membrane was evaluated by permeation flux (J, g/(m^2 h)), separation factor (α) and pervaporation separation index (PSI) calculated via the following equations:

$$J = \frac{Q}{A \times t} \quad (1)$$

$$\alpha = \frac{P_W / P_E}{F_W / F_E} \quad (2)$$

$$PSI = J \times (\alpha - 1) \quad (3)$$

where, Q is the mass of permeate (g) collected during a time interval of t (h), A is the effective membrane area in contact with feed solution (m^2). P and F represent the mass fractions of water (with the subscript W) or ethanol (with the subscript E) in the permeate and feed solutions, respectively. To guarantee the reliability of experimental data, three duplicated samples were fabricated under the same condition, and the pervaporation experiments for each sample were repeated for three times. The results of three samples were averaged as the final data.

3. Results and discussion

3.1. Morphologies of composite membranes

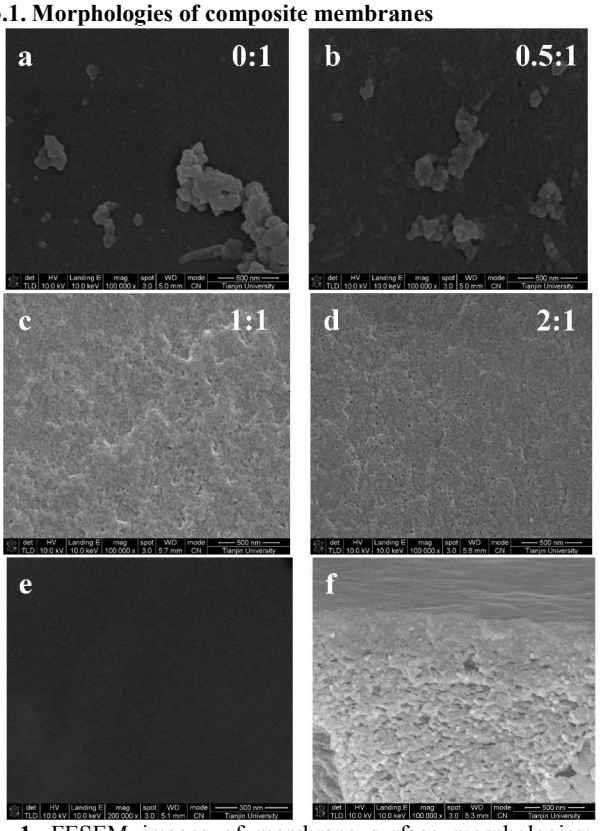

Fig. 1. FESEM images of membrane surface morphologies: (a) PDA(4 h)/PAN, (b) PEI-PDA(4 h, 0.5:1)/PAN, (c) PEI-PDA(4 h, 1:1)/PAN, (d) PEI-PDA(4 h, 2:1)/PAN, (e) SA/PEI-PDA(4 h, 1:1)/PAN; (f) FESEM image of SA/PEI-PDA(4 h, 1:1)/PAN membrane cross-section morphology.

The surface morphologies of PEI-PDA/PAN membranes with different mass ratios of PEI/DA were characterized by FESEM. In the absence of PEI, abundant sub-micron scale PDA aggregates appear on membrane surface (Fig. 1a), which gradually diminish and ultimately vanish with the introduction of PEI (Fig. 1b-d). During the deposition process of PDA, dopamine first transforms into 5,6-dihydroxyindole and 5,6-indolequinone through oxidation, intramolecular cyclization, and rearrangement, which further form oligomers such as trimer and tetramer through polymerization.[25-27] Afterwards, the oligomers stack and assemble into aggregates both in solution and on membrane surface *via* noncovalent interactions such as π-π stacking, hydrogen bond and charge transfer interactions. After introducing PEI in dopamine solution, the nucleophilic amine groups on PEI molecule can react with dopamine or other intermediates through Michael addition or Schiff base reactions and form PEI-PDA complex.[25, 26, 28] As a result, the structure and conformation of PDA oligomers are changed, thus disturbing the stacking and assembly of oligomers, and then inhibiting the formation of aggregates.[28, 29] However, the severe disturbance for oligomers arising from excessive PEI molecules in solution can decrease the deposition amount of PEI-PDA complex. When the mass ratio of PEI/DA increases to 2:1, abundant nanopores appear on membrane surface (Fig. 1d), indicating that the deposition amount of PEI-PDA complex is not enough to completely cover the PAN membrane. Compared Fig. 1c and e, it can be observed that the membrane possesses smooth surface without nanopores and aggregates after coating SA, indicating the complete coverage of SA for PEI-PDA/PAN membrane surface. The cross-section image of SA/PEI-PDA(4 h, 1:1)/PAN membrane in Fig. 1f shows that the separation layer tightly adheres to support layer without apparent boundary. This phenomenon can be ascribed to three reasons: dopamine and PEI molecules penetrate into the nanopores of PAN support layer during deposition process due to their relatively small size; slight pore penetration of SA occurs in the nanopores of PEI-PDA/PAN membrane; the ultrathin SA layer binds firmly with PEI-PDA/PAN membrane through abundant interaction sites.

3.2. Chemical properties of composite membranes

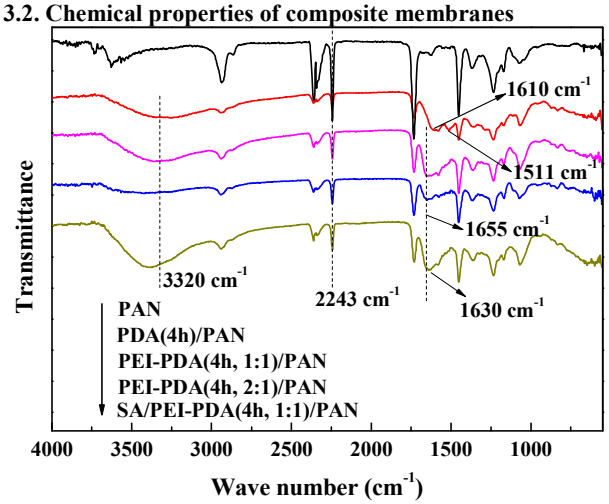

Fig. 2. FT-IR spectra of PAN, PEI-PDA(4 h, Y)/PAN and SA/PEI-PDA(4h, 1:1)/PAN membranes.

Various analysis methods including FT-IR, elemental analysis, zeta potential and water contact angle were employed to evaluate the effect of deposition condition on the chemical properties of PEI-

PDA(4 h, Y)/PAN membrane surfaces. After depositing PDA on PAN membrane surface, new peaks appear on FT-IR spectrum of PDA(4 h)/PAN membrane at 3320 cm^{-1}, 1610 cm^{-1} and 1511 cm^{-1} (Fig. 2), which can be ascribed to the stretching vibration of Ar-OH, stretching vibration of C=C in aromatic ring and bending vibration of N-H on PDA, respectively.[28, 30] The characteristic peak of –CN at 2243 cm^{-1} weakens due to the coverage of PDA for PAN membrane. The new peak at 1655 cm^{-1} on the spectra of PEI-PDA/PAN membranes belongs to the stretching vibration of C=N, confirming the Schiff base reaction between PEI and PDA.[26, 28] When the mass ratio of PEI/DA increases to 2:1, the reduced deposition amount of PEI-PDA complex leads to the significant weakening of absorption peaks at 3320 cm^{-1} and 1655 cm^{-1}. After coating SA as separation layer, the peak at 3300 cm^{-1}-3400 cm^{-1} strengthens due to the abundant hydroxyl and carboxyl groups on SA. Meanwhile, a new peak appears at 1630 cm^{-1} assigning to the antisymmetric stretching vibration of $–COO^-$.

Table 1 Surface chemical compositions and zeta potentials of PEI-PDA(4 h, Y)/PAN membranes.

Membrane	PEI/PDA (w/w)	Zeta potential (mV)
PDA(4 h)/PAN	-	-34.2±1.1
PEI-PDA(4 h, 0.5:1)/PAN	0.62	27.2±0.8
PEI-PDA(4 h, 1:1)/PAN	1.35	31.7±0.1
PEI-PDA (4 h, 2:1)/PAN	0.60	24.3±1.2

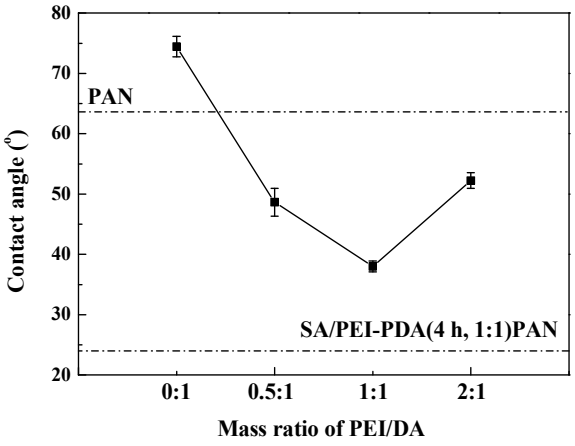

Fig. 3. Water contact angles on PEI-PDA(4 h, Y)/PAN membrane surfaces.

Various analysis methods including FT-IR, elemental analysis, zeta potential and water contact angle were employed to evaluate the effect of deposition condition on the chemical properties of PEI-PDA(4 h, Y)/PAN membrane surfaces. After depositing PDA on PAN membrane surface, new peaks appear on FT-IR spectrum of PDA(4 h)/PAN membrane at 3320 cm^{-1}, 1610 cm^{-1} and 1511 cm^{-1} (Fig. 2), which can be ascribed to the stretching vibration of Ar-OH, stretching vibration of C=C in aromatic ring and bending vibration of N-H on PDA, respectively.[28, 30] The characteristic peak of –CN at 2243 cm^{-1} weakens due to the coverage of PDA for PAN membrane. The new peak at 1655 cm^{-1} on the spectra of PEI-PDA/PAN membranes belongs to the stretching vibration of C=N, confirming the Schiff base reaction between PEI and PDA.[26, 28] When the mass ratio of PEI/DA increases to 2:1, the lessened deposition amount of PEI-PDA complex leads to the significant weakening of absorption peaks at 3320 cm^{-1} and 1655 cm^{-1}.

The final PEI/PDA mass ratio on membrane surface can be calculated as follows:

$$\mathrm{PEI/PDA(w/w)} = 0.281 \times \left(\frac{1 - 2\,\mathrm{N/C}}{8\,\mathrm{N/C} - 1}\right) \quad (4)$$

where, N/C is the atomic ratio of N and C elements obtained through elemental analysis. With the augment of PEI/DA mass ratio in deposition solution, the final PEI/PDA mass ratio on membrane surface increases at first and then decreases (Table 1), which arises from the discrepant deposition behaviours of PEI-PDA complexes with different compositions. The amount of PEI molecules participating Michael addition or Schiff base reactions with PDA and then forming PEI-PDA complex increases with the PEI/DA mass ratio. At lower PEI/DA mass ratio (≤ 1:1), the incorporation of PEI exerts indistinctive influence on the deposition of PEI-PDA complex, leading to the increase of final PEI/PDA mass ratio. At higher PEI/DA mass ratio (> 1:1), most of the PEI molecules in solution are prone to forming PEI-PDA complex containing extremely limited dopamine molecules and are inhibited to deposit on support layer surface, thus decreasing the final PEI/PDA mass ratio. PDA(4 h)/PAN membrane exhibits the zeta potential of -34.2 mV (Table 1) due to the negatively charged quinone groups.[31] Because of the abundant positive charges on PEI and the higher hydrophilicity of PEI compared with PDA, the zeta potential (Table 1) and water contact angle (Fig. 3) of PEI-PDA(4 h, Y)/PAN membranes exhibit variation trends in accordance with the final PEI/PDA mass ratio. Both the largest amount of positive charge and the highest hydrophilicity are obtained when the PEI/DA mass ratio is 1:1. Furthermore, the hydrophilicity of PEI-PDA/PAN membranes is much higher than that of PAN membrane, which is conducive to increasing the interfacial compatibility between separation layer and support layer,[6, 32] and decreasing the interfacial stress generated during the solvent evaporation process of separation layer.

3.3. Free volume properties of composite membranes

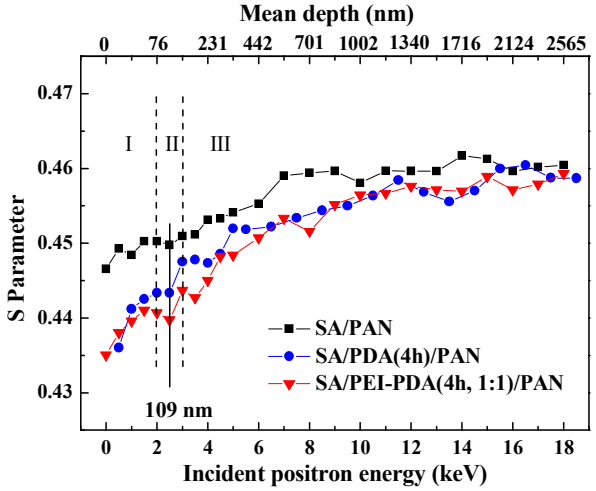

Fig. 4. *S* parameter as a function of the incident positron energy for SA/PAN, SA/PDA(4 h)/PAN and SA/PEI-PDA(4 h, 1:1)/PAN membranes.

In order to establish the correlations between interfacial interactions-membrane structure-separation performance, the slow positron annihilation Doppler broadening energy spectra were obtained to investigate the impact of interfacial interactions on the free volume properties of composite membrane. The incident positron energy determines the mean implantation depth of positrons in membranes, which can be calculated utilizing the following empirical equation,[33]

$$R_e = \left(\frac{40}{\rho}\right) E^{1.6} \quad (5)$$

where, R_e represents the mean implantation depth (nm), ρ is the density of membrane material (g/cm^3) and E is the positron energy (keV). According to the density of SA, the mean depths corresponding to different positron energies were obtained and listed in Fig. 4. The S parameter in Y axis indicates the information of cavities at a certain depth, which is defined as the ratio of the probed photon count within the range of 510.24-511.76 keV to that within the range of 504.2-517.8 keV. The reduction of S parameter suggests the decreased fractional free volume and increased membrane compactness. Therefore, the S-E curves in Fig. 4 can represent the free volume properties of membranes along with depth from membrane surface. All the S-E curves exhibit a slight reduction in the increasing process, which results from the more compact structure of interface region compared with adjacent domains.[32, 34, 35] Therefore, the location of interface can be ascertained at about 109 nm according to the S-E curves and the cross-section image of SA/PEI-PDA(4 h, 1:1)/PAN membrane in Fig. 1f. The S-E curves can be approximately divided into three sections—I: separation layer, II: interface region, III: support layer. By comparing the three curves, the order of membrane compactness in separation layer and interface region is obtained as follows: SA/PAN membrane < SA/PDA(4 h)/PAN membrane < SA/PEI-PDA(4 h, 1:1)/PAN membrane. As shown in Fig. S5a, the main interfacial interactions between separation layer and support layer in SA/PAN membrane are the weak hydrogen bonds between cyano groups on PAN and carboxyl/hydroxyl groups on SA. After depositing PDA on PAN membrane, the abundant hydroxyl/quinone/amino groups on PDA can form stronger hydrogen bonds with SA (Fig. S5b). For SA/PEI-PDA(4 h, 1:1)/PAN membrane, apart from the hydrogen bonds between PEI-PDA and SA, the protonated amino groups on PEI can form electrostatic attractions with carboxylates on SA (Fig. 5). In conclusion, the order of interfacial bonding strength in different composite membranes is: SA/PAN membrane < SA/PDA(4 h)/PAN membrane < SA/PEI-PDA(4 h, 1:1)/PAN membrane, which is in accordance with the order of membrane compactness. Therefore, it can be deduced that the free volume property and compactness of membrane are closely related to interfacial interactions.

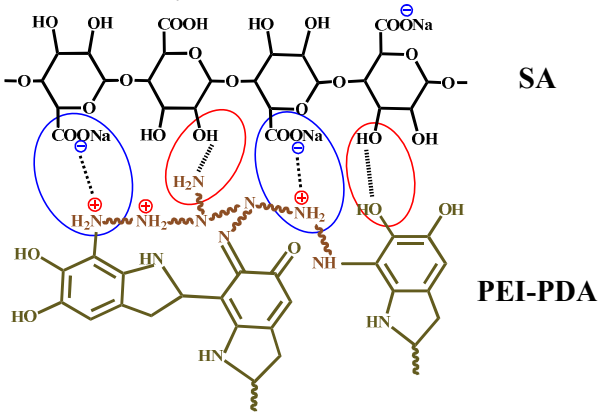

Fig. 5. Interfacial interactions in SA/PEI-PDA(4 h, 1:1)/PAN membrane.

3.4. Separation performance of composite membranes

3.4.1 Effect of PEI/DA mass ratio on separation performance

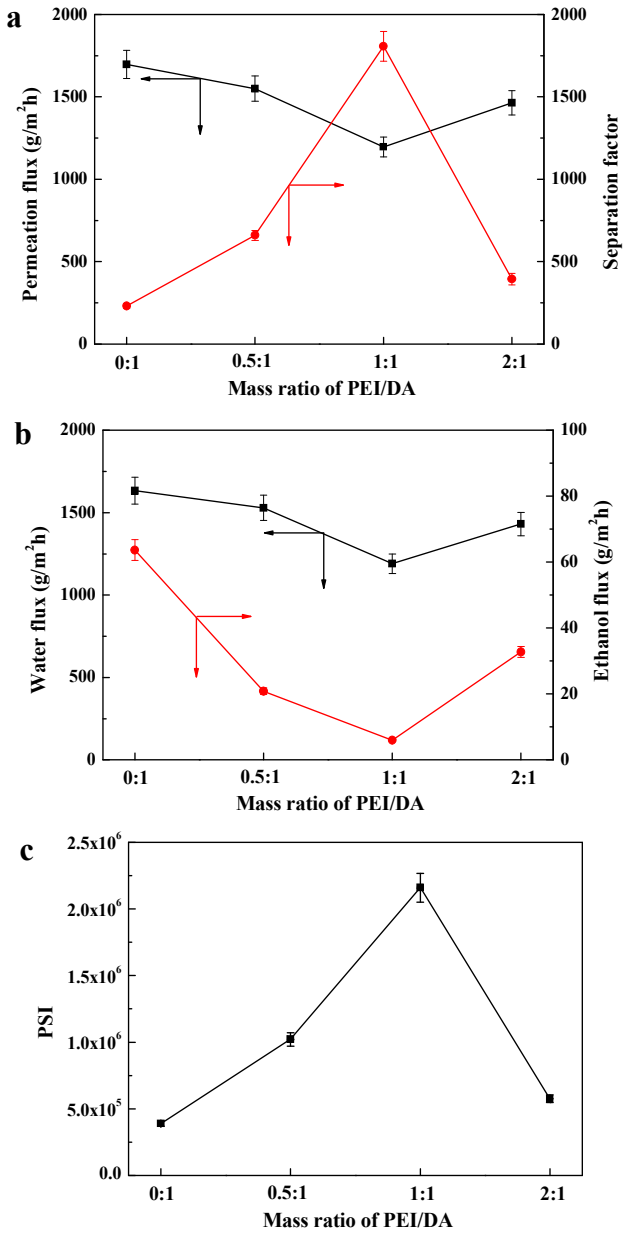

Fig. 6. Pervaporation performance of SA/PEI-PDA(4 h, Y)/PAN membranes: (a) permeation flux and separation factor, (b) water flux and ethanol flux, (c) PSI value.

The pervaporation experiments of SA/PEI-PDA(4 h, Y)/PAN membranes were performed with 90 wt% ethanol aqueous solution at 350 K to investigate the effect of PEI/DA mass ratio on separation performance. As shown in Fig. 6a, the separation factor increases dramatically at first and then decreases with the PEI/DA mass ratio increasing, while the permeation flux exhibits the opposite trend. The as-fabricated composite membrane shows the optimal performance at PEI/DA mass ratio of 1:1 with the permeation flux of 1196 g/(m^{2}h), the separation factor of 1807, and the PSI value of 2.16×10^6. On one hand, with the PEI/DA mass ratio augments from 0:1 to 1:1, the facilitated PEI deposition on support layer surface increases the interfacial interaction sites of electrostatic attraction (between PEI and SA). On the other hand, the covalent reaction between PEI and dopamine inhibits the oxidation and polymerization reactions between dopamine molecules, which

shifts the adhesion/cohesion balance of PDA to adhesion, and then increases interfacial interaction sites of hydrogen bond[23] (between PDA and SA). Meanwhile, the crosslinking effect of PEI for PDA offsets the decrease of PDA cohesive energy. The synergy of above factors leads to increscent membrane compactness and swelling resistance both in separation layer and interface region, which raise the diffusion resistance especially for ethanol molecules, and then increase diffusion selectivity for water. As a result, the ethanol flux steeply declines from 63.6 g/(m^{2}h) to 5.9 g/(m^{2}h) and the separation factor remarkably increases from 231 to 1807. With the further augment of PEI/DA mass ratio, the deposition amount of PEI and PDA on support layer surface lessens, leading to the decrease of interfacial interaction sites (both electrostatic attraction and hydrogen bond) and interfacial bonding strength. The resultant loose membrane structure weakens its sieving capacity for ethanol molecules. Therefore, the separation factor decreases dramatically at higher PEI/DA mass ratio. The water/ethanol separation performance of pristine and modified PAN membranes are also evaluated as listed in Table S1. Compared with PAN and PDA(4 h)/PAN membranes, PEI-PDA(4 h, 1:1)/PAN membrane exhibits enhanced separation factor for water permeation due to the partially covered nanopores on PAN membrane and the remarkably improved hydrophilicity after depositing PEI-PDA. However, the separation factor of PEI-PDA(4 h, 1:1)/PAN membrane is orders of magnitude lower than that of the SA/PEI-PDA(4 h, 1:1)/PAN membrane, confirming that the high separation factor of as-fabricated composite membrane is mainly attributed to SA separation layer and interface region.

3.4.2 Effect of deposition time on separation performance

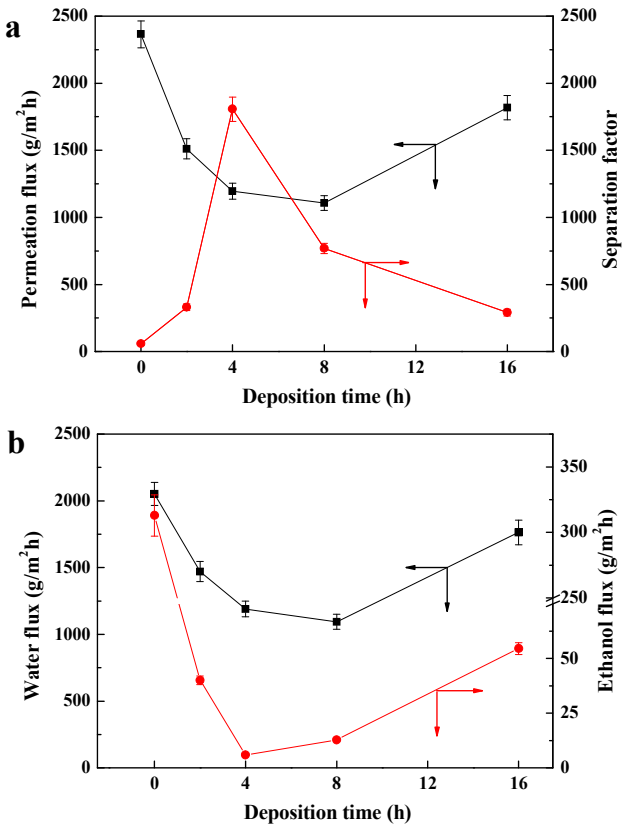

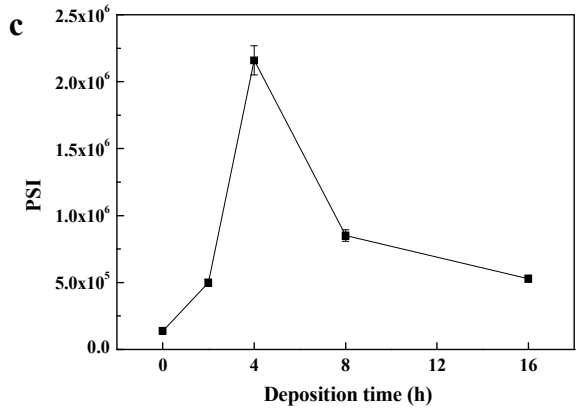

Fig. 7. Pervaporation performance of SA/PEI-PDA(X, 1:1)/PAN membranes: (a) permeation flux and separation factor, (b) water flux and ethanol flux, (c) PSI value.

The effect of deposition time on separation performance was investigated with 90 wt% ethanol aqueous solution at 350 K. Fig. 7a shows that the separation factor of SA/PEI-PDA(X, 1:1)/PAN membranes increases dramatically at first and then decreases after the deposition time is longer than 4 h. At the initial stage (≤ 4 h), the surface coverage of PEI-PDA complex for PAN membrane gradually augments with deposition time (Fig. S2), which adds the interfacial interaction sites of electrostatic attraction (Fig. S4) and hydrogen bond. As a result, the interfacial bonding strength increases, leading to the improved membrane compactness, swelling resistance, and diffusion selectivity for water. The ethanol flux decreases sharply from 313 g/(m^{2}h) to 5.9 g/(m^{2}h), while the separation factor increases from 59 to 1807. With the continuous increase of deposition time (> 4 h), the complete coverage for PAN membrane surface is achieved. Nevertheless, the surface chemical properties change due to the further reactions between PEI and PDA molecules as well as the reactions among PDA molecules. As a result, more amino groups on PEI are consumed,[20] leading to the decreased interfacial interaction sites of electrostatic attraction (Fig. S4). Meanwhile, the adhesion/cohesion balance of PDA shifts towards cohesion, thus decreasing interfacial interaction sites of hydrogen bond.[23] Consequently, the preferential diffusion of as-prepared composite membrane for water are weakened due to the decrescent interfacial bonding strength, resulting in the remarkable decrease of separation factor at higher deposition time.

3.4.3 Long-term separation performance

The long-term operation stability is crucial to the practical application of membrane. Fig. S7 shows the long-term separation performance of SA/PEI-PDA(4 h, 1:1)/PAN membrane up to 72 h for 90 wt% ethanol aqueous solution at 350 K. During the entire test, the permeation flux and water content in permeate fluctuate within a narrow range, implying the desirable structural stability of the composite membrane.

3.4.4 Comparison of the separation performance in this study with previous SA-based membranes in literatures

SA is an extensively utilized membrane material for pervaporation dehydration process because of its high water-affinity, excellent film-forming ability and various modification methods. Table 2 summarizes the separation performance of recently reported SA-based membranes for water/ethanol mixtures. Due to the ultrathin separation layer and the optimized membrane structure arising from interfacial interactions manipulation, the SA/PEI-PDA/PAN composite

membrane fabricated in this work shows high performance both in permeation flux and separation factor. The data in Table 2 are also plotted in Fig. S8 to acquire clearer comparison of membrane performance.

4.Conclusion

In summary, an efficient mussel-inspired approach to enhancing separation selectivity of composite membrane was explored via manipulating interfacial interactions between separation layer and support layer. Ultrathin composite membranes were fabricated by co-depositing biomimetic adhesive dopamine and PEI on support layer, then coating SA as separation layer. Both interaction effect and synergistic effect exist between dopamine and PEI molecules: (1) PEI reacts with dopamine during the formation process of PDA, thus anchoring PEI onto support layer surface; (2) the incorporation of PEI disturbs the stacking and assembly of PDA oligomers, thus affecting the deposition behaviour of PDA; (3) PDA and PEI form hydrogen bond interaction and electrostatic attraction interaction with SA respectively, which simultaneously impact the interfacial bonding strength. By regulating the deposition conditions of PEI-PDA complex, the chemical composition on support layer surface and the interfacial bonding strength are simultaneously manipulated to acquire optimal free volume property and swelling resistance of composite membrane, leading to the remarkably elevated selectivity. The highest separation factor of SA/PEI-PDA/PAN membranes for water/ethanol separation reaches 1807, which is 29.6 and 6.8-fold higher than those of SA/PAN and SA/PDA/PAN membranes, respectively. Considering the broad utilizations of composite membrane, this study may devote a facile and generic approach to fabricating high-selectivity membranes for diverse separation systems and membrane processes.

Table 2 Comparison of the separation performance in this study with previous SA-based membranes in literatures.

Membrane	Temperature (K)	Water content in feed (wt.%)	Thickness (μm)	Pervaporation performance			Reference
				Permeation flux (g/m^2h)	Separation factor	PSI (10^5)	
SA/PEI-PDA/PAN	350	10	0.1	1196[a]	1807[a]	21.6	This work
SA-HPA	303	4	40	43[a]	59976[a]	25.8	36
	303	4	40	70[a]	6291[a]	4.40	
	303	10	40	140[a]	14991[a]	21.0	
	333	10	40	315[b]	1000[b]	3.15	
SA-4A	298	2.5	43.5	106[a]	396[a]	0.42	37
	298	6.2	43.5	130[b]	90[b]	0.12	
SA-PTA	303	10	50	111[a]	1866[a]	2.07	38
	333	10	50	567[a]	220[a]	1.24	
SA-PVP-PWA	343	4	50	1500[b]	1000[b]	15.0	39
	300	10	50	100[b]	1250[b]	1.25	
SA-rGO/PAN	350	10	1.6	1699[a]	1566[a]	26.6	40
HA/SA/PAN	353	10	0.5	972[a]	1130[a]	11.0	41
SA/HA/PAN	353	10	0.5	948[a]	527[a]	4.99	
SA-PAA@Fe_3O_4/PAN	350	10	0.385	1634[a]	1044[a]	17.0	42

[a] Values are obtained directly from the data in references. [b] Values are estimated from the plots in references.

Acknowledgements

The authors gratefully acknowledge the financial support from the National Science Fund for Distinguished Young Scholars (No. 21125627), the National Natural Science Foundation of China (Nos. 21490583 and 21306131), Specialized Research Fund for the Doctoral Program of Higher Education (20120032120009), Seed Foundation of Tianjin University, and the Program of Introducing Talents of Discipline to Universities (No: B06006).

Notes and references

[a] Key Laboratory for Green Chemical Technology of Ministry of Education, School of Chemical Engineering and Technology, Tianjin University, Tianjin 300072, China. Fax: +86 22 23500086; E-mail: zhyjiang@tju.edu.cn

[b] Collaborative Innovation Center of Chemical Science and Engineering (Tianjin), Tianjin 300072, China.

[c] Multi-discipline Research Division, Institute of High Energy Physics, Chinese Academy of Sciences, Beijing 100049, China.

[d] Beijing Engineering Research Center of Radiographic Techniques and Equipment, Beijing 100049, China.

Electronic Supplementary Information (ESI) available: Photographs of membranes with different deposition conditions, morphology and chemical properties of membranes with different deposition times, interfacial interactions in SA/PAN and SA/PDA(4 h)/PAN membranes, separation performance of pristine and modified PAN membranes, effect of temperature on membrane separation performance, long-term separation performance, and comparison of membrane in this study with previous SA-based membranes in literatures. See DOI: 10.1039/c000000x/

1 K. Huang, G. P. Liu, Y. Y. Lou, Z. Y. Dong, J. Shen and W. Q. Jin, *Angew. Chem., Int. Ed.*, 2014, **53**, 6929-6932.
2 J. Zhao, X. T. Zhao, Z. Y. Jiang, Z. Li, X. C. Fan, J. N. Zhu, H. Wu, Y. L. Su, D. Yang, F. S. Pan and J. F. Shi, *Prog. Polym. Sci.*, 2014, **39**, 1668-1720.
3 D. L. Gin and R. D. Noble, *Science*, 2011, **332**, 674-676.
4 H. W. Kim, H. W. Yoon, S. M. Yoon, B. M. Yoo, B. K. Ahn, Y. H. Cho, H. J. Shin, H. Yang, U. Paik, S. Kwon, J. Y. Choi and H. B. Park, *Science*, 2013, **342**, 91-95.
5 W. Wei, S. S. Xia, G. P. Liu, X. H. Gu, W. Q. Jin and N. P. Xu, *AIChE J.*, 2010, **56**, 1584-1592.
6 J. Ma, M. H. Zhang, H. Wu, X. Yin, J. Chen, Z. Y. Jiang, *J. Membr. Sci.*, 2010, **348**, 150-159.
7 R. Y. M. Huang, P. Shao, *J. Membr. Sci.*, 2007, **287**, 162-179.
8 Y. F. Li, S. F. Wang, H. Wu, R. L. Guo, Y. Liu, Z. Y. Jiang, Z. Z. Tian, P. Zhang, X. Z. Cao and B. Y. Wang, *ACS Appl. Mater. Interfaces*, 2014, **6**, 6654-6663.
9 K.-H. Oh, M.-J. Choo, H. Lee, K. H. Park, J.-K. Park and J. W. Choi, *J. Mater. Chem. A*, 2013, **1**, 14484-14490.
10 G. M. Shi and T.-S. Chung, *J. Membr. Sci.*, 2013, **448**, 34-43.
11 J. Ma, M. H. Zhang, Z. Y. Jiang, M. C. Nie and G. X. Liu, *J. Membr. Sci.*, 2010, **364**, 290-297.
12 J. J. Wilker, *Angew. Chem., Int. Ed.*, 2010, **49**, 8076-8078.
13 J. H. Waite, N. H. Andersen, S. Jewhurst and C. Sun, *J. Adhes.*, 2005, **81**, 297-317.
14 J. H. Waite, *Nat. Mater.*, 2008, **7**, 8-9.
15 H. Lee, S. M. Dellatore, W. M. Miller and P. B. Messersmith, *Science*, 2007, **318**, 426-430.
16 X. Jiang, X. L. Yang, Y. H. Zhu, Y. F. Yao, P. Zhao and C. Z. Li, *J. Mater. Chem. A*, 2015, **3**, 2361-2369.
17 T. Lee, E. K. Jeon and B. S. Kim, *J. Mater. Chem. A*, 2014, **2**, 6167-6173.
18 F. Liu, F. Sun and Q. Pan, *J. Mater. Chem. A*, 2014, **2**, 11365-11371.
19 D. R. Dreyer, D. J. Miller, B. D. Freeman, D. R. Paul and C. W. Bielawski, *Chem. Sci.*, 2013, **4**, 3796-3802.
20 H. Lee, N. F. Scherer and P. B. Messersmith, *Proc. Natl. Acad. Sci. U. S. A.*, 2006, **103**, 12999-13003.
21 Q. Ye, F. Zhou and W. Liu, *Chem. Soc. Rev.*, 2011, **40**, 4244-4258.
22 H.-C. Yang, J. Luo, Y. Lv, P. Shen and Z.-K. Xu, *J. Membr. Sci.*, 2015, **483**, 42-59.
23 Y. F. Li, S. F. Wang, H. Wu, J. T. Wang and Z. Y. Jiang, *J. Mater. Chem.*, 2012, **22**, 19617-19620.
24 J. Zhao, F. S. Pan, P. Li, C. H. Zhao, Z. Y. Jiang, P. Zhang and X. Z. Cao, *ACS Appl. Mater. Interfaces*, 2013, **5**, 13275-13283.
25 V. Ball, D. Del Frari, M. Michel, M. Buehler, V. Toniazzo, M. Singh, J. Gracio and D. Ruch, *BioNanoSci.*, 2012, **2**, 16-34.
26 Y. Liu, K. Ai and L. Lu, *Chem. Rev.*, 2014, **114**, 5057-5115.
27 Y. Ding, L. T. Weng, M. Yang, Z. Yang, X. Lu, N. Huang and Y. Leng, *Langmuir*, 2014, **30**, 12258-12269.
28 H.-C. Yang, K.-J. Liao, H. Huang, Q.-Y. Wu, L.-S. Wan and Z.-K. Xu, *J. Mater. Chem. A*, 2014, **2**, 10225-10230.
29 H. C. Yang, J. K. Pi, K. J. Liao, H. Huang, Q. Y. Wu, X. J. Huang and Z. K. Xu, *ACS Appl. Mater. Interfaces*, 2014, **6**, 12566-12572.
30 R. N. Zhang, Y. L. Su, X. T. Zhao, Y. F. Li, J. J. Zhao and Z. Y. Jiang, *J. Membr. Sci.*, 2014, **470**, 9-17.
31 B. Yu, J. X. Liu, S. J. Liu and F. Zhou, *Chem. Commun.*, 2010, **46**, 5900-5902.
32 C. Zhao, H. Wu, X. Li, F. Pan, Y. Li, J. Zhao, Z. Jiang, P. Zhang, X. Cao and B. Wang, *J. Membr. Sci.*, 2013, **429**, 409-417.
33 P. J. Schultz and K. G. Lynn, *Rev. Mod. Phys.*, 1988, **60**, 701-779.
34 F. S. Pan, H. P. Jia, S. Z. Qiao, Z. Y. Jiang, J. T. Wang, B. Y. Wang and Y. R. Zhong, *J. Membr. Sci.*, 2009, **341**, 279-285.
35 B. Li, W. P Liu, Z. Y. Jiang, X. Dong, B. Y. Wang and Y. R. Zhong, *Langmuir*, 2009, **25**, 7368-7374.
36 V. T. Magalad, A. R. Supale, S. P. Maradur, G. S. Gokavi and T. M. Aminabhavi, *Chem. Eng. J.*, 2010, **159**, 75-83.
37 F. U. Nigiz, H. Dogan and N. D. Hilmioglu, *Desalination*, 2012, **300**, 24-31.
38 S. G. Adoor, V. Rajineekanth, M. N. Nadagouda, K. C. Rao, D. D. Dionysiou and T. M. Aminabhavi, *Sep. Purif. Technol.*, 2013, **113**, 64-74.
39 V. T. Magalad, G. S. Gokavi, C. Ranganathaiah, M. H. Burshe, C. Han, D. D. Dionysiou, M. N. Nadagouda and T. M. Aminabhavi, *J. Membr. Sci.*, 2013, **430**, 321-329.
40 K. T. Cao, Z. Y. Jiang, J. Zhao, C. H. Zhao, C. Y. Gao, F. S. Pan, B. Y. Wang, X. Z. Cao and J. Yang, *J. Membr. Sci.*, 2014, **469**, 272-283.
41 C. Y. Gao, M. H. Zhang, J. W. Ding, F. S. Pan, Z. Y. Jiang, Y. F. Li and J. Zhao, *Carbohydr. Polym.*, 2014, **99**, 158-165.
42 C. H. Zhao, Z. Y. Jiang, J. Zhao, K. T. Cao, Q. Zhang and F. S. Pan, *Ind. Eng. Chem. Res.*, 2014, **53**, 1606-1616.

The table of contents entry

Water/ethanol separation selectivity of composite membrane is remarkably elevated by manipulating interfacial interactions via mussel-inspired approach.

Authors: Jing Zhao, Chenhao Fang, Yiwei Zhu, Guangwei He, Fusheng Pan, Zhongyi Jiang,* Peng Zhang, Xingzhong Cao and Baoyi Wang

Title: Manipulating the interfacial interactions of composite membrane via mussel-inspired approach toward enhanced separation selectivity

TOC Figure